3464 *Biochemistry* **2010,** *49,* 3464–3476
DOI: 10.1021/bi902178w

BIOCHEMISTRY
including biophysical chemistry & molecular biology
Article

Structures of Human Carbonic Anhydrase II/Inhibitor Complexes Reveal a Second Binding Site for Steroidal and Nonsteroidal Inhibitors[†,‡]

Gyles E. Cozier,[§] Mathew P. Leese,[§] Matthew D. Lloyd,[§] Matthew D. Baker,[∥,⊥] Nethaji Thiyagarajan,[∥] K. Ravi Acharya,[∥] and Barry V. L. Potter*[,§]

[§]*Medicinal Chemistry, Department of Pharmacy and Pharmacology and* [∥]*Department of Biology and Biochemistry, University of Bath, Claverton Down, Bath BA2 7AY, United Kingdom* [⊥]*Present address: School of Biosciences, Cardiff University, Cardiff CF10 3AX, United Kingdom*

Received December 18, 2009; Revised Manuscript Received March 4, 2010

ABSTRACT: Carbonic anhydrase (CA) catalyzes the reversible hydration of carbon dioxide to hydrogen carbonate, and its role in maintaining pH balance has made it an attractive drug target. Steroidal sulfamate esters, inhibitors of the cancer drug target steroid sulfatase (STS), are sequestered *in vivo* by CA II in red blood cells, which may be the origin of their excellent drug properties. Understanding the structural basis of this is important for drug design. Structures of CA II complexed with 2-methoxyestradiol 3-*O*-sulfamate (**3**), 2-ethylestradiol 3,17-*O*,*O*-bis(sulfamate) (**4**), and 2-methoxyestradiol 17-*O*-sulfamate (**5**) are reported to 2.10, 1.85, and 1.64 Å, respectively. Inhibitor **3** interacts with the active site Zn(II) ion through the 3-*O*-sulfamate, while inhibitors **4** and **5** bind through their 17-*O*-sulfamate. Comparison of the IC_{50} values for CA II inhibition gave respective values of 56, 662, 2113, 169, 770, and 86 nM for estrone 3-*O*-sulfamate (**1**), 2-methoxyestradiol 3,17-*O*,*O*-bis(sulfamate) (**2**), **3**, **4**, **5**, and 5′-((4*H*-1,2,4-triazol-4-yl)methyl)-3-chloro-2′-cyanobiphenyl-4-yl sulfamate (**6**), a nonsteroidal dual aromatase−sulfatase inhibitor. Inhibitors **2**, **5**, and **6** showed binding to a second adjacent site that is capable of binding both steroidal and nonsteroidal ligands. Examination of both IC_{50} values and crystal structures suggests that 2-substituents on the steroid nucleus hinder binding via a 3-*O*-sulfamate, leading to coordination through a 17-*O*-sulfamate if present. These results underline the influence of small structural changes on affinity and mode of binding, the degree of flexibility in the design of sulfamate-based inhibitors, and suggest a strategy for inhibitors which interact with both the active site and the second adjacent binding site simultaneously that could be both potent and selective.

Carbonic anhydrase (CA; EC 4.2.1.1) is a Zn(II)-dependent enzyme that catalyzes the reversible hydration of carbon dioxide into hydrogen carbonate and a proton and plays an important role in physiological anion-exchange processes and fluid balance (*1*). This enzyme has long been a drug target for the treatment of glaucoma (*2*, *3*) but has taken on new importance recently as a potential target for obesity (*4*) and cancer (*5*, *6*) (see ref *7* for a comprehensive review). CA isoforms can also catalyze a series of other hydration and dehydration reactions, although it is not clear whether these reactions have any physiological significance in normal or cancerous cells (*7*). At present 16 isoforms of CA have been identified in vertebrates, with all but one identified in humans. These isoforms have different physiological and pathological roles, and they can be localized in the cytosol (CA I−III, VII, and XIII) or mitochondria (CA VA and VB), whereas others are secreted (CA VI) or are membrane-bound and have extracellular active site domains (CA IV, IX, XII, and XIV) (*2*). The CA XV isoform has recently been reported to be expressed in rodents and other higher vertebrates but not in humans or other primates (where it is encoded by a pseudogene) (*8*). There is convincing evidence for the overexpression of CA isoforms IX and XII in cancer (see, e.g., ref *9*), and this is supposed to promote growth of a tumor by acidification of the extracellular environment. Expression is upregulated under hypoxic conditions, which is common in solid tumors (*10*, *11*).

The phenolic sulfamate ester group has proven to be a key pharmacophore in a range of both enzyme inhibitors (*12*, *13*) and microtubule disrupting agents (*14*−*16*) and one which delivers beneficial effects on both the activity and the drug-like properties of the molecules into which it is incorporated (*14*). Our interest in compounds bearing the phenolic sulfamate moiety stems from a program on the design of inhibitors of steroid sulfatase (STS),[1] a key enzyme for the production of circulatory estrogen in postmenopausal women and therefore a candidate (and now clinical) target for the treatment of hormone-dependent tumors (*17*, *18*). We reported the first clinical trial of such an STS inhibitor recently (*18*), and this compound STX64 (also known as BN83495) is currently in several phase I and II trials in breast, endometrial, and prostate cancer. Initial medicinal chemistry

[†]This work was funded by Sterix Ltd., a member of the Ipsen group.
[‡]Coordinates and structure factors have been deposited with the Protein Data Bank (accession codes CA II/inhibitor **3** 2x7u.pdb, CA II/inhibitor **4** 2x7t.pdb, and CA II/inhibitor **5** 2x7s.pdb).
*To whom correspondence should be addressed [+44-1225-386639 (phone); +44-1225-386114 (fax); B.V.L.Potter@bath.ac.uk (e-mail)].

[1]Abbreviations: CA II, human carbonic anhydrase II; EMATE, estrone 3-*O*-sulfamate; 2-MeOE2bisMATE, 2-methoxyestradiol 3,17-*O*,*O*-bis(sulfamate); STS, steroid sulfatase; E2, estradiol; E2S, estradiol sulfate; DASI, dual aromatase−steroid sulfatase inhibitor.

 Published on Web 03/18/2010

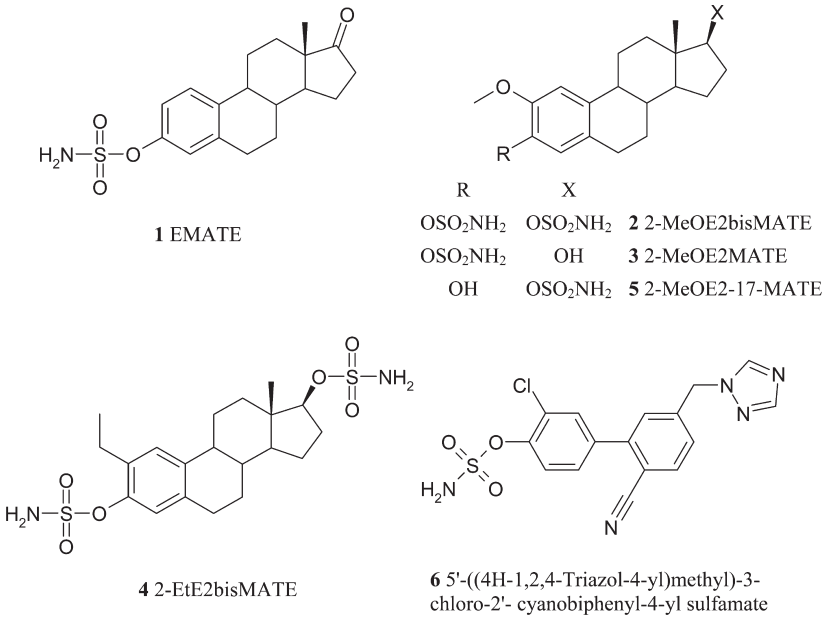

FIGURE 1: Structures of EMATE (**1**), 2-MeOE2bisMATE (**2**), and inhibitors **3**, **4**, **5**, and **6**.

considerations envisaged that the ionizable sulfamate group ($-OSO_2NH_2$), like a range of phosphonate and thiophosphonate groups, might serve as a suitable isostere for the sulfate (SO_3^-) group of the natural STS substrate estradiol sulfate (E2S), and thus a range of sulfamoylated estrogen derivatives was synthesized for evaluation as potential STS inhibitors. The prototypical compound in this series, estrone 3-*O*-sulfamate (EMATE), proved to be a potent inhibitor of STS with an IC_{50} for the conversion of radiolabeled E2S to estradiol (E2) in the low nanomolar range (*12*, *19*, *20*). Furthermore EMATE, in addition to its high activity, proved to be the first irreversible inhibitor of STS (*20*) and, unusually for an estrogen derivative, the compound displayed excellent oral bioavailability (*13*) and pharmacokinetics (*21*, *22*). Although elucidation of the precise mechanism of STS inhibition by sulfamate-based inhibitors has proven elusive, the origins of their excellent properties *in vivo* appear to be linked to their almost complete uptake by red blood cells after oral administration and consequent bypassing of first pass liver metabolism (*21*, *22*). This effect appears to stem from the reversible interaction of such sulfamate esters with the catalytic site of carbonic anhydrase II, an enzyme highly expressed in red blood cells, through a coordination of the monoanionic form of the aryl sulfamate moiety to the Zn(II) ion (*5*, *6*).

We have also described the beneficial effects of a phenolic sulfamate group on the activities of 2-substituted estrogen-derived microtubule disruptors, wherein the group contributes to enhancements in activity, metabolic stability, and oral bioavailability (*14*). Investigation of the interaction of the clinical development candidate 2-methoxyestradiol 3,17-*O*,*O*-bis(sulfamate) (2-MeOE2bisMATE) with CA II by protein crystallography revealed, in addition to an unexpected interaction with the catalytic Zn(II) ion through the aliphatic C-17 sulfamate group rather than the aryl sulfamate, the presence of a possible second ligand binding site in the large lipophilic pocket above the catalytic site (*23*). This result was intriguing in terms of the potential effects of the C-2 substituent adjacent to the phenolic sulfamate and its influence on coordination geometry and the extent to which this may direct coordination of the ligand to the catalytic site. We were particularly curious to investigate the potential generality of this second ligand binding site and whether other related compounds might give similar complexes. Some crystal structures of CA II have also shown a second zinc binding site located on the surface of the protein interacting with His-4, His-64, and His-36 of a symmetry-related molecule (*24*, *25*). It was suggested that this second zinc binding site is involved in stabilizing the crystal packing interactions. Herein, we describe three new CA II−ligand protein structures: with the steroid sulfamate-based inhibitors 2-methoxyestradiol 3-*O*-sulfamate (Figure 1, inhibitor **3**), 2-ethylestradiol 3,17-*O*,*O*-bis(sulfamate) (Figure 1, inhibitor **4**), and 2-methoxyestradiol 17-*O*-sulfamate (Figure 1, inhibitor **5**), crystals of which diffracted to 2.10, 1.85, and 1.64 Å, respectively. Also, the novel nonsteroidal biphenyl-based dual aromatase−sulfatase inhibitor 5′-((4*H*-1,2,4-triazol-4-yl)methyl)-3-chloro-2′-cyanobiphenyl-4-yl sulfamate (Figure 1, inhibitor **6**), briefly reported previously (*26*), is described in more detail, particularly its second inhibitor binding site which is also observed in the structure of CA II in complex with inhibitor **5**.

EXPERIMENTAL PROCEDURES

Materials. All chemicals and reagents were purchased from the Sigma-Aldrich Chemical Co. or Fisher Ltd. and were of analytical grade or higher and were used without further purification. Plasmid pACA encoding for human CA II was obtained from Professor C. Fierke (University of Michigan) and was grown and purified as previously described (*24*). Inhibitors **3**−**6** (Figure 1) were synthesized as previously described (*23*, *26*, *27*). GE Healthcare provided protein chromatography systems and columns.

Measurement of IC_{50} Values and Dissociation Constants. In order to assess the inhibition of carbonic anhydrase *in vitro*, an adaptation of a colorimetric assay previously developed was used (*28*). CA-catalyzed hydrolysis of *p*-nitrophenyl acetate produces *p*-nitrophenol which has an absorption peak at 348 nm which allows for colorimetric determination of product and subsequent calculation of enzyme activity.

Inhibition constants (IC_{50} values) were measured based on the method previously described (*6*) using a 96-well plate

Table 1: X-ray Data Collection and Refinement Statistics[a]

	inhibitor **3**	inhibitor **4**	inhibitor **5**
(A) data statistics			
space group	$P2_12_12_1$	$P2_1$	$P2_12_12_1$
no. of molecules/asymmetric unit	1	1	1
cell dimensions			
a, *b*, *c* (Å)	42.50, 69.54, 73.21	42.26, 40.83, 72.7	42.04, 71.92, 73.75
α, *β*, *γ* (deg)	$\alpha = \beta = \gamma = 90$	$\alpha = \gamma = 90, \beta = 104.5$	$\alpha = \beta = \gamma = 90$
resolution range (Å)	50−2.12 (2.21−2.12)	40.93−1.89 (1.95−1.89)	50−1.64 (1.70−1.64)
R_{sym}[a] (%)	6.7 (37.6)	4.9 (11.6)	6.2 (35.1)
$I/\sigma(I)$	15.2 (2.8)	18.8 (7.7)	19.7 (2.3)
completeness (%)	82.0 (42.1)	96.9 (99.3)	92.3 (63.7)
total no. of reflections	117892	131202	452628
no. of unique reflections	12877	19429	28009
redundancy	2.2 (2.0)	1.4 (1.4)	4.5 (2.3)
Wilson *B*-factor (Å^2)	27.6	15	22.1
no. of water molecules	73	107	137
(B) refinement statistics			
resolution range (Å)	50−2.12	40.93−1.89	50−1.64
R_{cryst} (%)	19.8	21.1	25.6
R_{free} (%)	25.3	24.8	27.7
rmsd in bond lengths (Å)	0.006	0.007	0.008
rmsd in bond angles (deg)	1.3	1.4	1.4
Ramachandran plot statistics			
most favored (%)	95.3	95.7	94.8
additionally allowed (%)	4.7	4.3	5.2
generously allowed (%)	0.0	0.0	0.0
disallowed (%)	0.0	0.0	0.0
overall average *B*-factor (Å^2)			
protein	27.4	16	23.6
primary Zn^{2+}	14.8	11	12.2
secondary Zn^{2+}	43.7	80.1	47.3
primary ligand	49.9	19.3	23.3
secondary ligand	none	none	24.3
glycerol	54.5	39.5	46.7
water	34.8	22.1	30

[a]Values in parentheses are for the highest resolution shell.

spectrophotometric assay, except that the initial rates were measured rather than the absorbance after 20 min. Assays contained human CA II (Sigma, 180 nM) and 1 mM 4-nitrophenol acetate in 50 mM Tris-HCl, pH 7.6, in a final volume of 0.20 mL. Initial rates of the enzyme-catalyzed reaction were monitored for 2 min at 20 °C. Stock solutions and dilutions of inhibitors were prepared in ethanol such that there was a constant 5% ethanol in the assay. At least three replicants at each concentration were used.

Inhibitor dissociation constants for inhibitors **3**−**6** were determined as previously described using human CA II (Sigma) (*24*). Final concentrations of enzyme and 4-nitrophenyl acetate substrate in the assay were at 180 nM and 3 mM, respectively. Final concentrations of inhibitors in the assays were 1.5, 3, 4.5, 6, and 7.5 μM for **3**, 0.1, 0.25, 0.5, 0.75, and 1 μM for **4**, 0.25, 0.75, 1.25, 2.5, and 3.75 μM for **5**, and 25, 50, 100, 150, and 200 nM for **6**.

Crystallization, Data Collection, and Structural Determination. The hanging drop vapor diffusion method was used for crystallization. Protein (2.5 μL, ∼10 mg/mL, ∼0.3 mM) containing 0.5 mM inhibitors and 30 mM 2-mercaptoethanol was mixed with well buffer (2.5 μL; 0.1 M Tris-HCl, pH 8.0, 1 mM $ZnSO_4$, and 2.49 M ammonium sulfate), with crystals appearing after 3−4 weeks at 4 °C.

X-ray diffraction data were collected under cryogenic conditions at the Synchrotron Radiation Source (Daresbury, U.K.) station PX14.2 for inhibitor **3**, station PX9.6 for inhibitor **4**, and station X13 at DESY (Hamburg, Germany) for inhibitor **5**. Before data collection the crystals were flash-cooled to 100 K in a cryoprotectant containing the reservoir solution and 33% (v/v) 8 M sodium formate. Data were indexed and reduced with DENZO and SCALEPACK modules of the HKL suite (*29*) in the $P2_12_12_1$ space group for inhibitors **3** and **5** and orthorhombic $P2_1$ space group for inhibitors **4** and **6**. The structures were determined by molecular replacement with Phaser (*30*) using CA II crystallized in either the $P2_12_12_1$ space group (1TTM.pdb) (*24*) or the $P2_1$ space group (1CA2.pdb) (*31*) as the starting models (all nonprotein data were removed from the starting models before use). Refinement was performed using CNS (*32*−*34*) in addition to manual model building using the program Coot (*35*). Clear density for the active site zinc and the inhibitors was observed after the first round of refinement for each CA II/inhibitor complex. For each complex the zinc and inhibitor were introduced into the active site. The topology files for each inhibitor were generated using the Hic-up Server (*36*). Where applicable, the second zinc and inhibitor molecules were introduced. After alternating cycles of water addition, refinement, and manual rebuilding the final inhibitor **3** complex had an $R_{free} = 25.3$ and $R_{cryst} = 19.8$, the inhibitor **4** complex had a final $R_{free} = 24.8$ and $R_{cryst} = 21.1$, and the inhibitor **5** complex had a final $R_{free} = 27.7$ and $R_{cryst} = 25.6$ (Table 1).

Table 2: IC_{50} Values and Equilibrium Dissociation (K_i) Constants[a]

inhibitor	CA II IC_{50} (nM)		K_i (nM)
	previous study using end point	this study using initial rate	
1, EMATE	23 ± 12	56 ± 10	nd
2, 2-MeOE2bisMATE	379	662 ± 86	nd
3, 2-methoxyestradiol 3-*O*-sulfamate	376	2113 ± 256	5340 ± 833
4, 2-ethylestradiol 3,17-*O*,*O*-bis(sulfamate)	290	169 ± 31	232 ± 57
5, 2-methoxyestradiol 17-*O*-sulfamate	549	770 ± 51	1660 ± 177
6, 5′-((4*H*-1,2,4-triazol-4-yl)methyl)-3-chloro-2′-cyanobiphenyl-4-yl sulfamate	21	86 ± 8	31 ± 8

[a] IC_{50} values (end point (*6*, *25*) and initial rate experiments) and equilibrium dissociation (K_i) constants for the inhibitors of human CA II. Structures of the tested inhibitors are shown in Figure 1. nd = not determined.

RESULTS

Assays and Measurement of IC_{50} Values and Dissociation Constants. The esterase activity of human carbonic anhydrase II was assayed using the reported spectrophotometric assay containing 4-nitrophenyl acetate as the substrate and forms the basis of activity inhibition by potential CA II inhibitors. EMATE, the benchmark inhibitor, was previously shown to have an IC_{50} of 23 nM (*25*) (Table 2), consistent with other reported values of 42 nM (*6*, *37*) and 10 nM (*5*). Inhibition of activity by 2-MeOE2bisMATE and inhibitors **3**−**6** (Figure 1) was also previously assessed by this assay (Table 2) (*6*). Inhibitor **4** proved to be the most potent of the steroid sulfamate-based inhibitors with an IC_{50} of 290 nM. 2-MeOE2bisMATE and inhibitor **3** were almost identical with IC_{50} values of 379 and 376 nM, respectively. Inhibitor **5** had the highest IC_{50} value of 549 nM, and inhibitor **6** had an IC_{50} value of 21 nM, which is very similar to that of EMATE. As these IC_{50} values had been measured at different times, although they were all obtained with acetazolamide as a standard inhibitor, it was decided for a better comparison to repeat the experiment so that all of the inhibitors could be tested with the same batch of enzyme. Also, the assay used previously was based on an end point concentration of product (absorbance measured after 30 min), whereas it is generally considered that the initial rate of the enzyme reaction should be used. Under these assay conditions EMATE has an IC_{50} of 56 nM, and inhibitor **6** is again similar with an IC_{50} of 86 nM. These values are higher than those measured using the end point assay, as are those for 2-MeOE2bisMATE and inhibitor **5** (IC_{50} of 662 and 770 nM, respectively). In these assays **4** again proved to be the most potent of the 2-substituted steroid sulfamate-based inhibitors with an IC_{50} of 169 nM, which is in fact a lower value than that measured using the end point assay. In general, although the values measured in the two assays differ, their relative affinities are consistent with those measured previously. The exception to this is the IC_{50} value measured for inhibitor **3** which is significantly different to that measured before. Here, the IC_{50} for inhibitor **3** measured is 2113 nM, a >5 fold increase on that measured previously and no longer similar to that obtained for 2-MeOE2bisMATE.

In this study, to further characterize the binding by CA II, we have also determined the equilibrium dissociation constant for inhibitors **3**−**6** (Table 2). These are consistent with the IC_{50} value measured in each case, with **6** having the lowest value of 31 nM. Of the steroid-based inhibitors, **4** has the lowest equilibrium dissociation constant of 232 nM, with **5** having a value of 1660 nM and **3** of 5340 nM.

*Overall Structures of Inhibitors **3**, **4**, **5**, and **6** in Complex with Carbonic Anhydrase*. Cocrystallization of CA II with inhibitors **3**, **4**, **5**, and **6** produced crystals of the enzyme−inhibitor complex, with structures containing inhibitors **3** and **5** in the $P2_12_12_1$ space group and those with inhibitors **4** and **6** in the $P2_1$ space group. These are the two space groups which CA II crystals have previously been reported to adopt (*38*, *39*), and the overall structure of CA II in these space groups is similar. As expected, the maps for all of the structures showed strong positive density for the active site Zn(II) ion ligated by the three active site histidine residues (His-94, -96, and -119). During the early stages of refinement the presence of the inhibitors in the binding site was identified by strong positive density in the $|F_o| - |F_c|$ map corresponding to a sulfamate group within 2.5 Å of the active site Zn(II) ion. The inhibitor **3** and **5** complexes contain a second Zn(II) ion located near the entrance to the active site, as previously observed for some other CA II/inhibitor complexes that also crystallized in the $P2_12_12_1$ space group (*24*, *25*). The inhibitor **4** complex, which crystallized in the $P2_1$ space group, also showed a Zn(II) ion in this second binding site. The final models were produced by addition of the inhibitor molecules, Zn(II) ions, and water molecules with manual rebuilding and further refinement using CNS and Coot (Table 1). As mentioned, the overall backbone structures of the inhibitor **3**, **4**, **5**, and **6** complexes are very similar (Figure 2), and they are also similar to that of CA II without any ligand bound (PDB 1CA2), as shown by the rms deviations for Cα atoms being 0.41, 0.29, 0.46, and 0.30 Å, respectively.

Second Zinc Binding Site. CA II crystallizing in the $P2_12_12_1$ space group has been shown to sometimes contain a second zinc binding site on the surface of the protein coordinated to His-64, one or two water molecules, and His-36 from a symmetry-related molecule (*24*, *25*). As the zinc is bound by a symmetry-related molecule, it has been suggested that this second binding site is involved in the stabilization of crystal-packing interactions. CA II crystallized in the $P2_1$ space group usually contains a water molecule bonded to His-64 in an equivalent position to the second zinc binding site. Also, as it is in a different space group, the symmetry-related molecules are not in the same area to provide His-36 to form the site.

The CA II complexes with inhibitors **3** and **5** crystallize in the $P2_12_12_1$ space group, and they both contain the second zinc binding site (Figure 3). The second Zn(II) ion in the CA II inhibitor **3** complex has interactions with His-64 and His-36 from the symmetry-related molecule. Additionally, unlike the previously reported structures, there is an interaction with His-4. In the CA II inhibitor **5** complex there are clear interactions with His-4 and His-64. His-36, meanwhile, is poorly defined and perhaps does not form such a strong interaction as previously observed. The CA II complexes with inhibitors **4** and **6** crystallize

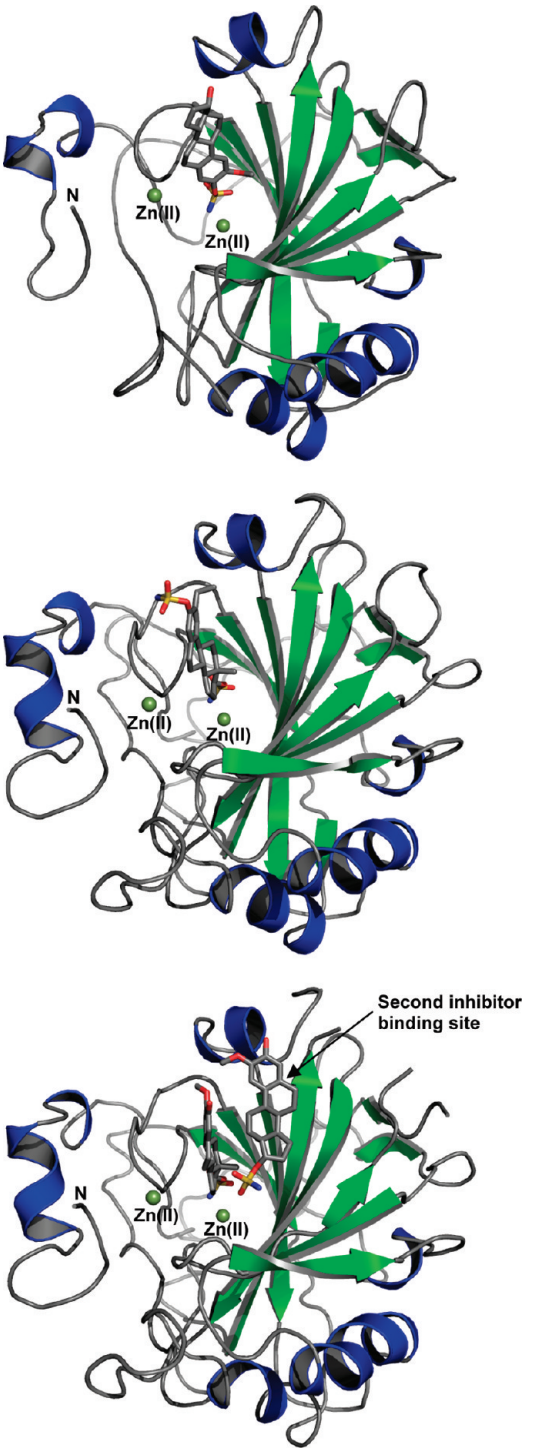

FIGURE 2: Ribbon diagrams showing the overall structures of the CA II inhibitor complexes. Secondary structure element α-helices are shown in blue and β-sheets in green. Bound inhibitor molecules are shown as sticks, and bound Zn(II) ions are shown as spheres in dark green. The N-terminus is labeled N, with the C-terminus obscured at the back of the structure. This diagram was prepared using PyMOL (http://www.delanoscientific.com).

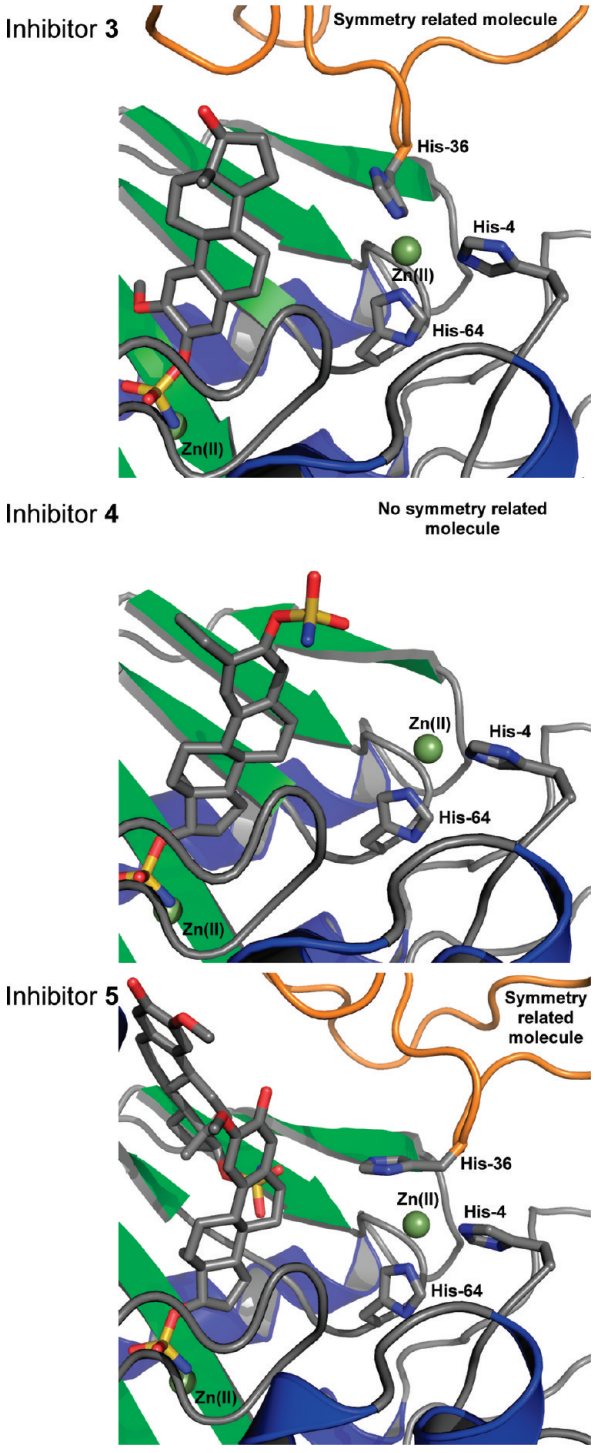

FIGURE 3: Close-up of the secondary zinc binding site of human CA II found in the inhibitor **3**, inhibitor **4**, and inhibitor **5** complexes. Secondary structure element α-helices are shown in blue and β-sheets in green. For the inhibitor **3** and inhibitor **5** complexes the secondary Zn(II) ion is bound by His-4, His-64, and His-36 from the symmetry-related molecule (shown as orange coil). The active site Zn(II) ion and bound inhibitors are included to indicate the position of the secondary Zn(II) ion in the overall structure. This diagram was prepared using PyMOL (http://www.delanoscientific.com).

in the $P2_1$ space group. However, the second zinc binding site was only seen for inhibitor **4**, and the coordinating residues are His-4 and His-64. His-36 (from the symmetry-related molecule as observed in the $P2_12_12_1$ space group) is not involved in zinc coordination due to different crystal packing.

Binding of Steroid Sulfamate Inhibitors in the Active Site of CA II. The $2|F_o| - |F_c|$ map for inhibitor **3** contoured at 1.0σ (Figure 4A) highlights that the density for the sulfamate group is clear, but there is only weak density for some of the steroid backbone, although there is density visible for almost all of the inhibitor with the contour level set to 0.7σ. The $2|F_o| - |F_c|$ and $|F_o| - |F_c|$ annealed omit maps also clearly show density for the sulfamate group and only weak density for the steroid backbone

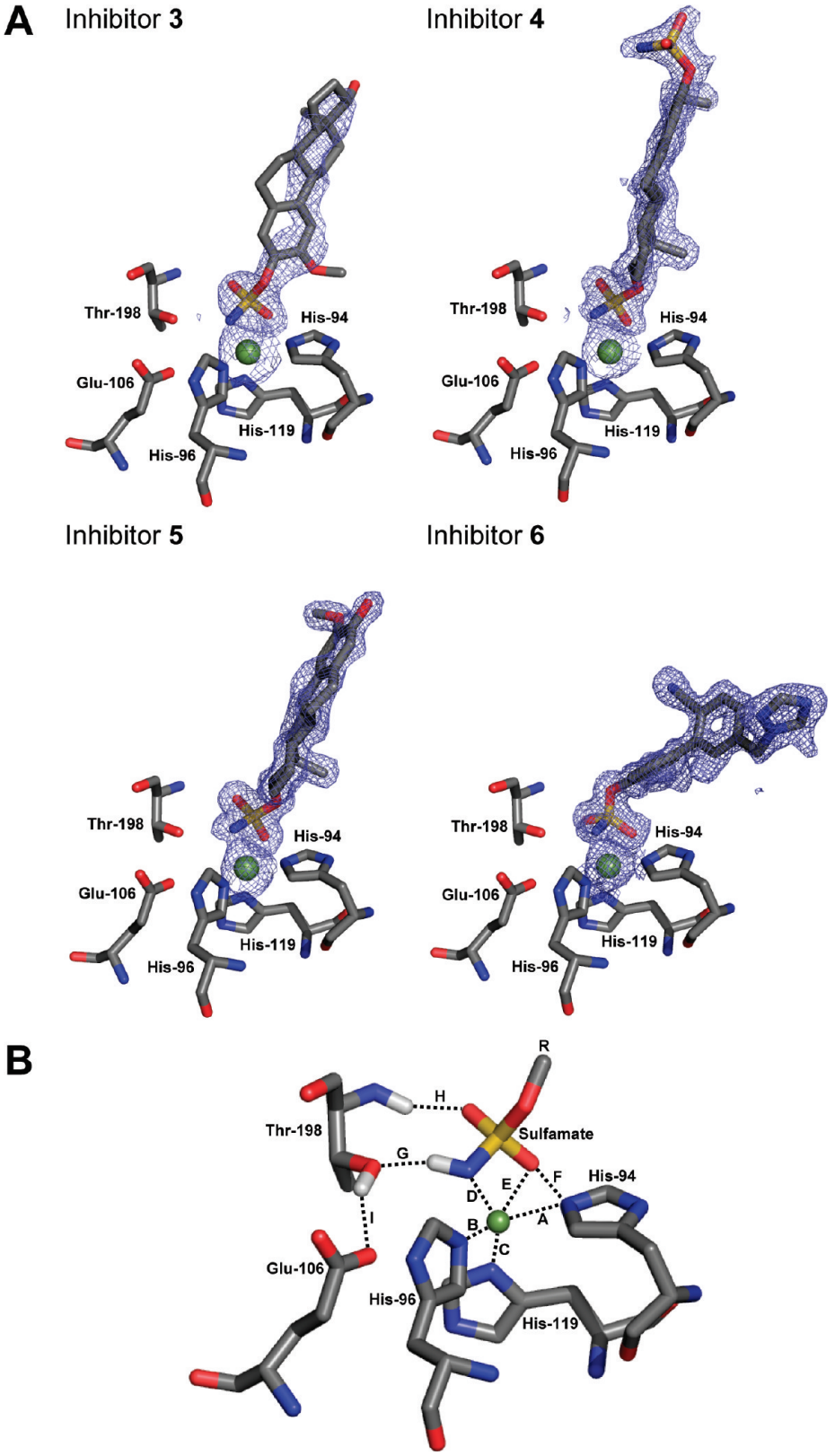

FIGURE 4: (A) Binding of inhibitors **3**, **4**, **5**, and **6** in the active site of human CA II showing density for the $2|F_o| - |F_c|$ map (blue) contoured at 1.0σ. (B) Important interactions that stabilize binding of sulfamate-containing inhibitors. The sulfamate and coordinating residues are shown as sticks, and the Zn(II) ion is shown as a dark green sphere. R denotes the rest of the inhibitor molecule. The lengths of these interactions are shown in Table 3. This diagram was prepared using PyMOL (http://www.delanoscientific.com).

(Supporting Information, Figure 1). Along with the *B*-values for the inhibitor this suggests a degree of flexibility in the orientation of the steroid backbone. Also, the inhibitor was modeled with an occupancy of 0.8. The $2|F_o| - |F_c|$ map for inhibitor **4** contoured at 1.0σ shows density for the whole inhibitor molecule (Figure 4A). However, as observed for 2-MeOE2bisMATE (*23*), the 3-*O*-sulfamate group is not as well-defined as the rest of the inhibitor molecule and could only

Table 3: Important Interactions That Stabilize Binding of Inhibitors

			distance in inhibitor complexes (Å)					
interaction[a]	first residue and atom	second residue and atom	inhibitor **1**	inhibitor **2**	inhibitor **3**	inhibitor **4**	inhibitor **5**	inhibitor **6**
A	His-94 NE2	Zn	2.00	2.01	2.19	2.16	2.02	1.97
B	His-96 NE2	Zn	2.03	2.03	2.23	2.25	1.99	2.04
C	His-119 ND1	Zn	2.00	2.05	2.05	2.18	1.97	2.05
D	inhibitor SO_3NH	Zn	1.78	1.93	1.93	2.14	2.14	1.96
E	inhibitor SO_3NH O2	Zn	3.30	3.15	3.14	3.13	3.16	2.92
F	inhibitor SO_3NH O2	His-94 NE2	3.54	3.75	3.41	3.62	3.68	3.28
G	inhibitor SO_3NH	Thr-198, side chain OH	2.69	2.75	2.86	2.63	2.77	2.78
H	inhibitor SO_3NH O1	Thr-198, main chain NH	2.79	3.01	2.90	3.03	2.99	2.97
I	Glu-106 OE1	Thr-198, side chain OH	2.53	2.58	2.63	2.49	2.56	2.57

[a]See Figure 4B for diagram showing these interactions.

be modeled with an occupancy of 0.5 (the rest of the inhibitor was modeled with 100% occupancy). This probably derives from the flexibility of this group, as it has at best only long-range water-mediated interactions with the protein molecule. Density for all of the molecule is clearly visible in the $2|F_o| - |F_c|$ and $|F_o| - |F_c|$ annealed omit maps (Supporting Information, Figure 1). The majority of inhibitor **5** is well-defined in the $2|F_o| - |F_c|$ map contoured at 1.0σ, with only parts of the A-ring density not observed, and was modeled with 100% occupancy (Figure 4A). Density for the majority of the molecule is visible in the $2|F_o| - |F_c|$ and $|F_o| - |F_c|$ annealed omit maps; as usual there is strong density for the sulfamate group bound to the zinc (Supporting Information, Figure 1).

The active site Zn(II) ion, as observed in previous structures, is bound by three histidines (His-94, His-96, and His-119) at the bottom of the active site funnel. The fourth coordination to the Zn(II) ion, which is a hydroxyl ion/water molecule in the native enzyme, is formed from the nitrogen of the sulfamate group of the inhibitors (Zn−N bond). Additionally, one of the oxygen atoms of the sulfamate group has a long distance interaction to the Zn(II) ion (Zn−O interaction). All of the interactions between the sulfamate group, the Zn(II) ion, and the protein are shown in Figure 4B, and the distances are reported in Table 3. EMATE and other steroid-based inhibitors that have been cocrystallized with CA II possess a 3-*O*-sulfamate group that has been shown to be coordinated to the zinc as the monoanion in the X-ray crystal structures. However, the recently reported structure of 2-MeOE2bisMATE in complex with CA II, where the ligand also contains an aliphatic 17-*O*-sulfamate ester group as well as an aryl 3-*O*-sulfamate ester group, gave the unexpected result that the 17-*O*-sulfamate group is coordinated to the zinc, instead of the usual 3-*O*-sulfamate. Of the inhibitors examined here **3** only has a 3-*O*-sulfamate group, while **5** only contains a 17-*O*-sulfamate group, and their modes of interaction are unambiguous. Inhibitor **4**, like 2-MeOE2bisMATE, contains both a 3-*O*-sulfamate and a 17-*O*-sulfamate group with the protein crystal structure revealing that coordination through the 17-*O*-sulfamate group is favored.

The steroid skeleton of all three steroid sulfamate inhibitors is orientated toward the hydrophobic region of the active site funnel, such that it can form many strong hydrophobic interactions with residues Gln-92, Val-121, Phe-130, Val-134, Leu-197, Thr-199, Pro-201, and Leu-203 (Figure 5). For inhibitors **4** and **5** the position and orientation of the steroid backbone are very similar to those of 2-MeOE2bisMATE, wherein the side edge of the steroid is orientated toward the hydrophobic region. The steroid backbone for inhibitor **4** and 2-MeOE2bisMATE overlay very closely, not surprising given their similarity, whereas for inhibitor **5** there is a small difference in the angle of the ligand in the active site. This has the effect that, even though the sulfamate and D-ring of the steroid backbone overlay very well, there is up to a 1.90 Å difference in the position of parts of the A-ring at the entrance to the active site funnel. There are no obvious additional interactions between inhibitor **4** and the hydrophobic region of CA II that could account for its increased affinity for CA II when compared with 2-MeOE2bisMATE, although the ethyl group of **4** is intrinsically more hydrophobic than the polar methoxy group of 2-MeOE2bisMATE. The similarity in the position and orientation of these three inhibitors (2-MeOE2bisMATE, **4**, **5**) is consistent with them all interacting with the zinc through the 17-*O*-sulfamate group.

In contrast, the orientation of inhibitor **3** which interacts via the 3-*O*-sulfamate group is significantly different to the other steroidal inhibitors, with the steroidal backbone positioned closer to the hydrophobic region of the active site funnel. In this structure the β-face of the steroid is directed toward the hydrophobic region rather than the edge as seen for the other inhibitors. Binding via the 3-*O*-sulfamate, as seen for inhibitor **3**, causes a greater than 1 Å shift of Phe-130 and a small shift of Val-134, when compared to the structures of inhibitors **4** and **5**, presumably resulting in maximization of hydrophobic interactions. A comparison of the inhibitor **3** complex with that of EMATE, which also interacts with CA II via its 3-*O*-sulfamate group, shows that the orientation of the steroid rings is in the same plane (with the face of the steroid rings orientated toward the hydrophobic region), yet the steroidal backbones are rotated 180° with respect to each other (thus the α- and β-faces are orientated toward the hydrophobic region for EMATE and **3**, respectively). This means that only the A- and C-rings of the steroid backbone overlay each other and the B- and D-rings do not overlay at all. This difference in coordination would logically derive from the presence of the 2-substituent in **3** which hampers optimal interaction with respect to EMATE, and this results in the observed reduction in inhibitory activity.

*Binding of Inhibitor **6** by CA II*. Inhibitor **6** was refined with an occupancy of 0.8, and there was almost complete density for each part of the ligand structure in the final model (Figure 4A). Density for most of the molecule is also clearly visible in the $2|F_o| - |F_c|$ and $|F_o| - |F_c|$ annealed omit maps (Supporting Information, Figure 1). There are several water molecules in the active site funnel located on either side of the inhibitor. There were also three areas of positive density in the $|F_o| - |F_c|$ map

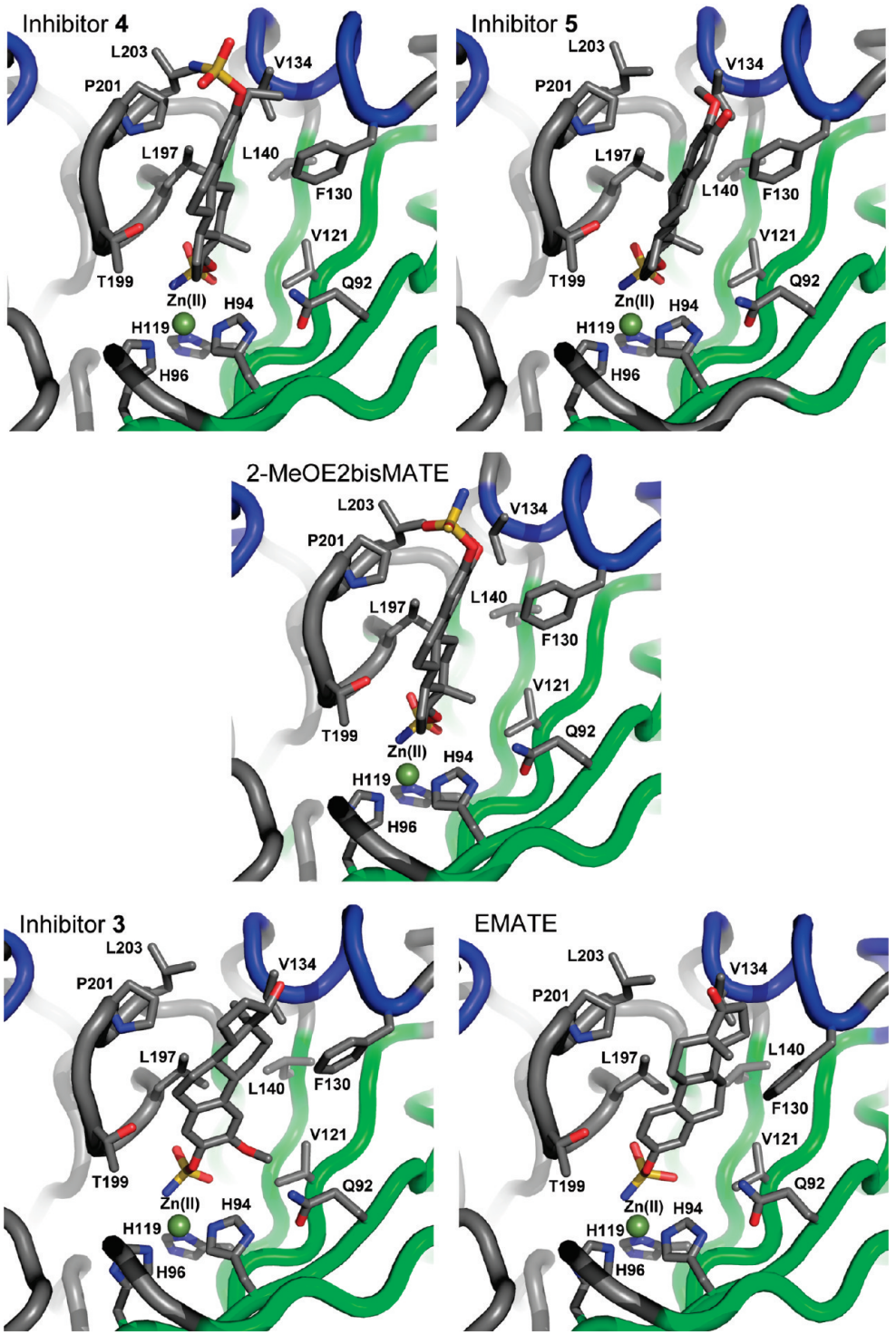

FIGURE 5: Detail of the hydrophobic interactions between 2-MeOE2bisMATE, EMATE, and inhibitors **3**, **4**, and **5** with CA II. The inhibitors and hydrophobic residues surrounding the steroid backbone of the inhibitors are shown as sticks; α-helical regions are shown in blue and β-sheets in green. The same orientation of the structure is shown for all inhibitors to highlight the side edge (inhibitors **4**, **5**, and 2-MeOE2bisMATE) or face (inhibitor **3** and EMATE) orientation of the steroid rings toward the hydrophobic region. This diagram was prepared using PyMOL (http://www.delanoscientific.com).

within 1.5 Å of the inhibitor which, although being similar in intensity to what would be expected for water molecules, were far too close to be modeled as such. With the occupancy of inhibitor **6** refined as 0.8, all three areas of positive density could correspond to waters in those molecules of the protein that do not have inhibitor **6** bound in the active site.

The active site Zn(II) ion, as observed in previous structures, is bound by three histidines (His-94, His-96, and His-119) at the bottom of the active site funnel. The Zn(II) ion is also coordinated to inhibitor **6** via the nitrogen of the sulfamate group, with a Zn−N distance of 1.96 Å, and a weaker interaction to one of the oxygen atoms from the sulfamate group (Zn−O distance of 2.92 Å). The sulfamate group is additionally bound to CA II by hydrogen bonds from the proton of the nitrogen atom to the hydroxyl group of Thr-198 and the second oxygen of the sulfamate to the backbone amide of Thr-198. The hydroxyl

group of Thr-198 also is hydrogen bonded to the Glu-106 carboxyl (Figure 4B). These hydrogen bonds and interactions of the Zn(II) ion and sulfamate group are generally conserved in all complexes of sulfamate-containing inhibitors with CA II.

The biphenyl group of inhibitor **6** is located coming out of the center of the funnel. Many inhibitors, including EMATE (*5*, *6*), 667-Coumate (STX64, BN83495) (*24*), and the steroid sulfamate inhibitors discussed in this study, have a significant degree of hydrophobic interaction with residues from the hydrophobic side of the funnel. With inhibitor **6** bound more toward the center of the funnel only the aromatic ring containing the sulfamate substituent, being at the narrow bottom of the funnel, is close enough to any of these hydrophobic residues to form meaningful interactions of which residues Val-121, Phe-130, and Leu-197 are the closest.

The triazole ring is nearest to the entrance of the active site funnel and is orientated toward the hydrophilic side in a small cleft formed by Leu-60, Asn-62, and Glu-69 and, in addition, Glu-237 of a symmetry-related molecule is located directly above this cleft in the crystal structure. There are two possible orientations of the triazole ring in this cleft, where the difference between these two orientations involves a 180° rotation of the ring. In the first orientation, the 2-N atom of the triazole ring would be 3.45 Å from Asn-62, and the 4-N atom of the triazole 3.13 Å from the backbone nitrogen of Glu-237 from a symmetry-related molecule. In the second orientation the 2-N atom of the triazole ring is 3.54 Å from Glu-69, and the 4-N atom of the triazole is 3.58 Å from the side-chain oxygen of Glu-237 from a symmetry-related molecule. These distances are all too long for optimal hydrogen bonding. From the electron density of inhibitor **6**, it is not possible to conclude which orientation is adopted or whether it is a mixture of the two orientations, but the first orientation does have the shorter distances, in particular the 3.13 Å distance between the triazole and the symmetry-related Glu-237, and therefore may be the predominant orientation in the crystal structure. It is also worth noting that in solution there would be no symmetry molecule; therefore, there is only the possibility of one hydrogen bond from either Asn-62 or Glu-69 that could anchor the triazole in this cleft, but the fact that the triazole ring could have an interaction with CA II in either orientation may help to increase the affinity of CA II for inhibitor **6**.

Second Inhibitor Binding Site. The recently reported structure of CA II in complex with 2-MeOE2bisMATE showed a previously unobserved second inhibitor binding site lying close to the surface at the entrance to the active site funnel. It was concluded that this may be a low-affinity site, only having an occupancy of 0.61, and therefore may be due to the high inhibitor concentration used in the crystallization.

During the refinement of the structure of CA II in complex with inhibitor **5** density for a second inhibitor molecule was also observed in the $2|F_o| - |F_c|$ map contoured at 1.0σ and the $2|F_o| - |F_c|$ and $|F_o| - |F_c|$ annealed omit maps contoured at 1.0σ and 3.0σ, respectively. At this contour level the density for the whole inhibitor molecule could be seen, and the inhibitor was modeled with an occupancy value of 1 without any negative density appearing in the $|F_o| - |F_c|$ map. However, the *B*-values for this second inhibitor were higher than for the active site inhibitor molecule. Using an occupancy value of 0.6 meant that the *B*-values were then in the same range as for the rest of the molecule, so it is likely that it represents also a lower affinity site as observed for the 2-MeOE2bisMATE/CA II complex. This second site for inhibitor **5** occupies the same position

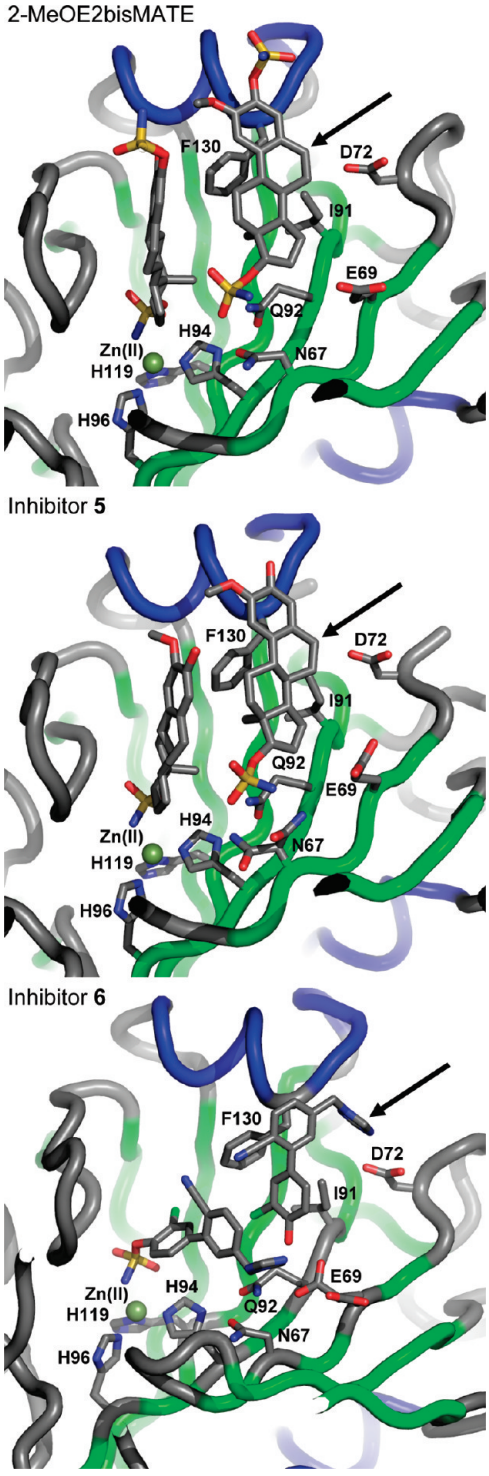

FIGURE 6: Second inhibitor binding site in human CA II. The position of the second inhibitor binding site (indicated by the arrow) near the entrance of the active site funnel is shown for 2-MeOE2-bisMATE and inhibitors **5** and **6**. Inhibitors and residues are shown as sticks; α-helical regions are shown in blue and β-sheets in green. This diagram was prepared using PyMOL (http://www.delanoscientific.com).

and orientation as the second site for 2-MeOE2bisMATE (Figure 6), although there is a difference in the orientation of the 17-*O*-sulfamate group. In the inhibitor **5**/CA II complex there is a dual conformation of Asn-67, with one conformation the same as that observed in the 2-MeOE2bisMATE CA II complex and forming a H-bond with the 17-*O*-sulfamate group of inhibitor **5** at a distance of 2.73 Å. The other Asn-67

conformation is positioned such that it can form two interactions with the 17-*O*-sulfamate group of inhibitor **5** with distances of 2.63 and 3.09 Å. So it appears that there may be a conformational change in the side chain of Asn-67 upon inhibitor binding in the second site. There is also a H-bond interaction between the 17-*O*-sulfamate group and Asn-62 at a distance of 2.80 Å, and longer range interactions between the 17-*O*-sulfamate group and Gln-92 (3.43 Å), and the 3-hydroxyl group of inhibitor **5** with Asp-129 (3.29 Å) and the main-chain nitrogen of Gly-131 (3.18 Å). There are also hydrophobic interactions with Ile-91, Gln-92, and Phe-130.

Examination of the same region in the $2|F_o| - |F|$ and $|F_o| - |F|$ maps for inhibitors **3** and **4**, although showing some small areas of weak density, revealed nothing resembling ring structures. Therefore, there is no evidence of a second binding site under the conditions used.

The second binding site of inhibitor **6** was observed on closer examination of the electron density maps while refining areas of unassigned positive density. When the inhibitor was introduced into the model structure with an occupancy of 0.75, clear electron density was observed for every part of the molecule apart from the sulfamate group in the $2|F_o| - |F_c|$ map. As the crystals were grown in an aqueous environment over a period of 4−6 weeks, it is possible that a percentage of the inhibitor molecules could have hydrolyzed to the corresponding phenol over the period of the crystallization. This is known for aryl sulfamates (*40*−*42*). The sulfamate group did not model well into the electron density maps; instead, the density in the region where the sulfamate group could be positioned models well as a second conformation for Glu-69 where it can interact with the hydroxyl group of inhibitor **6** formed by the hydrolysis of the sulfamate group. Possibly, the sulfamate group is too flexible to be clearly observed, or only inhibitor molecules with the sulfamate group hydrolyzed are able to bind in the second site, or alternatively there is a mixed population of inhibitor molecules with and without the sulfamate group.

This second site is on the surface of the protein at the entrance to the active site funnel and is at a similar position to the second binding site observed in the CA II/2-MeOE2bisMATE and CA II/inhibitor **5** complexes (Figure 6). Since 2-MeOE2bisMATE and **5** are structurally very similar (only missing the aryl-linked sulfamate) and inhibitor **6** is a biphenyl derivative, it is not too surprising that the orientation of inhibitor **6** in the second binding site is different. Hydrogen bonding from the triazole ring to the backbone nitrogen of Phe-130 and water-mediated hydrogen bonding to Asp-72 are observed along with hydrophobic interactions of the biphenyl group with Phe-130, Ile-91, and the one aryl ring of the inhibitor **6** molecule in the primary active site binding site. The gross structural details of the **6**/CAII complex were discussed briefly in Woo et al. (*26*).

DISCUSSION

Correlation of CA II/Steroid Sulfamate Inhibitor Complex Structures with Affinity. With the recent CA II/2-MeOE2bisMATE complex structure showing the unexpected result of coordination of 2-MeOE2bisMATE to the active site Zn(II) ion being via the 17-*O*-sulfamate, this posed the question of what factors might affect the relative affinity of ligands bound via either the 3-*O*- or 17-*O*-sulfamates. In principle, binding via the more acidic 3-*O*-sulfamate might be expected to be favored *a priori* since this will present substantially in the favored anionic form, whereas the aliphatic 17-*O*-sulfamate would either need to be deprotonated first before binding or, as is the case with water binding to CA to generate the catalytic hydroxyl-Zn anion, the neutral form may bind and then a proton be lost. So either binding of 2-MeOE2bisMATE to CA II via the 17-*O*-sulfamate must allow extra interactions that could not form if 2-MeOE2-bisMATE bound via the 3-*O*-sulfamate or binding via the 3-*O*-sulfamate would introduce unfavorable steric clashes. The crystal structures of CA II/inhibitor **3**, **4**, and **5** complexes and IC_{50} measurements reported in this study give some insights into this and the different interactions that affect the affinity of inhibitors for CA II.

A comparison of the CA II/inhibitor **3** (a 3-*O*-sulfamate derivative) and inhibitor **5** (a 17-*O*-sulfamate derivative) complexes confirms that both 3-*O*- and 17-*O*-sulfamate derivatives can interact with the active site zinc. The relative IC_{50} values for these inhibitors (2113 and 770 nM, respectively) show that in this case the binding via a less hindered, but less acidic, 17-*O*-sulfamate reveals a higher affinity. Comparison of the IC_{50} values for inhibitor **3** with that for EMATE (2113 and 56 nM respectively), where there is no possibility for the ligand to bind in any alternate fashion, shows the dramatic reduction in affinity when a methoxy group adjacent to the sulfamate is introduced. The reduced activity is thus likely due to steric hindrance caused by the 2-substituent that impedes optimal interaction of sulfamate and Zn(II) ion. When an inhibitor contains a 2-substituent, as well as 3-*O*- and 17-*O*-sulfamates (2-MeOE2bisMATE and inhibitor **4**), it is therefore not surprising that the crystal structures reveal binding via the 17-*O*-sulfamate group. The steroid-based inhibitors containing both 3-*O*- and 17-*O*-sulfamates are able to bind via either group; therefore, the IC_{50} value will be affected by changes in affinity of both sulfamate groups. The CA II/inhibitor complex crystal is likely to form with the most favorable orientation as the inhibitor will spend most of the time bound in that way. In line with this steric argument is our recent observation that simple dual aromatase−sulfatase inhibitors with a large bromo group substitution *ortho* to the sulfamate on a phenyl ring show reduced affinity for CA II over the unsubstituted scaffold (137 vs 27 nM, respectively) (*25*).

It has been reported that there is some correlation between the Zn−N distance (zinc to sulfamate nitrogen) and affinity, where high-affinity inhibitors supposedly have a shorter Zn−N distance (*5*). For example, previously observed Zn−N distances are usually in the range of 1.95−2.10 Å, but EMATE (a high-affinity inhibitor of CA II with a IC_{50} of 56 nM as described above) has a short Zn−N distance of 1.78 Å (*5*). As the bond between sulfamate nitrogen and Zn(II) ion is usually not the only interaction between inhibitor and CA II, then the Zn−N distance will only be an indication of how well an inhibitor fits into the bottom of the active site funnel to maximize all of its interactions with CA II. Comparing the relative Zn−N distances for the complexes with EMATE, 2-MeOE2bisMATE, and inhibitors **3**, **4**, and **5** (Table 3) shows that all of the steroid sulfamate-based inhibitors have a longer Zn−N bond length than EMATE. This is especially the case for inhibitors **4** and **5** with their obvious relatively different coordination to EMATE. However, 2-MeOE2bisMATE also binds via the 17-*O*-sulfamate, and its Zn−N distance is much shorter than that for inhibitors **4** and **5**, and the same as for inhibitor **3**, which binds the same way as EMATE via the 3-*O*-sulfamate. This longer Zn−N distance for the steroid sulfamate inhibitors is consistent with the higher IC_{50} values compared to EMATE (Table 2), although inhibitor **3** has

the equal shortest Zn−N distance of all the steroid sulfamate inhibitors but has the lowest affinity. Also, comparison between the 2-substituted steroid sulfamate inhibitors themselves does not completely correlate with the end point IC_{50} values. Furthermore, when the Zn−N distances and initial rate IC_{50} values are compared, there is very little correlation. The Zn−N distance of the potent CA II inhibitor **6** illustrates why this value cannot be solely used as a prediction of affinity, since **6** is equipotent to EMATE (as shown by both the end point and initial rate IC_{50} values), yet its complex has a significantly longer Zn−N bond length (1.96 Å for **6** and 1.78 Å for EMATE). Therefore, how tightly an inhibitor binds to CA II cannot be predicted solely based on the Zn−N distance. For example, there is also a longer range interaction between the zinc and one of the oxygens of the sulfamate group (Zn−O distance, Table 3). For EMATE this is quite long at 3.30 Å, but the very short Zn−N distance accounts for its high affinity. For the steroid-based inhibitors, the Zn−O interaction has a more important role with shorter distances of 3.15, 3.14, 3.13, and 3.16 Å for 2-MeOE2bisMATE and inhibitors **3**, **4**, and **5**, respectively. Although the Zn−O distance for inhibitor **4** is the shortest for the steroid-based inhibitors, the differences between the values are very small so this is unlikely to account for its higher affinity compared to the other inhibitors studied here. It could be that a change from a 2-MeO group to the more lipophilic 2-Et group may increase the affinity of binding via the 3-*O*-sulfamate group of these steroid derivatives.

It therefore appears that although Zn−N distance gives an indication of the affinity of some inhibitors for CA II, for predicting the relative affinities of the 2-substituted steroid sulfamate inhibitors for CA II use of the Zn−N distance is overly simplistic. Furthermore, inhibitor **6** also does not follow this trend as it is a high-affinity inhibitor, yet has a relatively long Zn−N distance. Thus, although a short Zn−N distance indicates that an inhibitor fits well into the bottom of the active site funnel to maximize all of its interactions and therefore likely has a high affinity for CA II, for inhibitors with a longer Zn−N distance then, it is not possible to predict their affinity for CA II based on that distance alone.

Second Inhibitor Binding Site. The observation of a second 2-MeOE2bisMATE binding site in the CA II structure led us to explore whether other steroid sulfamate inhibitors could also bind to this region of CA II. The clear evidence for a second inhibitor **5** molecule binding to the same region of CA II, as observed for the second 2-MeOE2bisMATE, and that the steroid backbone of both inhibitors overlays very closely (Figure 6), shows that the site is not specific. So this site does appear to be capable of binding a range of inhibitors, albeit probably being of lower affinity than that observed for binding in the active site.

Furthermore, the complex of CA II and **6** also shows binding of a second inhibitor molecule. It is interesting that this second binding site for inhibitor **6** is in an equivalent position to those observed in the complexes with 2-MeOE2bisMATE and inhibitor **5** (Figure 6). This suggests that this region of the protein surface is particularly suited for binding relatively hydrophobic compounds. The CA II complexes with 2-MeOE2bisMATE and inhibitor **6** both crystallized in the $P2_1$ space group, whereas the CA II complex with inhibitor **5** crystallized in the $P2_12_12_1$ space group. Therefore, the second binding site is not dependent on what space group is adopted. Also, as there are no interactions between the inhibitors bound in the second site and the symmetry-related molecule, this suggests this second binding site may not be an artifact of crystallization.

There have been previous reports of inhibitors binding to two sites on the CA II molecule. First, in a crystal structure, two molecules of phenol were shown bound to CA II (*43*), with one molecule near the bottom of the active site funnel (but not coordinated to the zinc), and the second molecule was bound close to the second inhibitor binding site shown in this study, but slightly further away from the active site funnel. Second, a study of fluoroaromatic−fluoroaromatic interactions using a variety of fluoroaromatic inhibitors showed that a second molecule of some of these inhibitors could bind to Phe-130 → Val CA II but not to the wild-type enzyme (*44*). The first inhibitor molecule is coordinated with the active site zinc in the usual way, and the second inhibitor molecule is located in the same region as the second inhibitor binding site from this study. The fluoroaromatic regions of the two inhibitors interact, with the rest of the second inhibitor molecule orientated across the second inhibitor binding site from this present study such that the phenylsulfonamide of the second fluoroaromatic inhibitor is located in the same area as the second phenol molecule in the CA II-phenol$_2$ structure.

More recently, structures of CA II in complex with so-called "two-prong" inhibitors containing benzenesulfonamide and IDA-Cu^{2+} groups also showed a second inhibitor binding site (*45*). This second site is located near the N-terminus, that is on the outside surface of the rim of the active site funnel, and is almost directly opposite the second binding site from this present study. Interestingly, the authors showed these inhibitors to be bound to this site in solution as well as in the crystal.

Evidence for second inhibitor binding sites could be of significant interest to drug design, not only for design relevant to CA II inhibition but perhaps in relation to the now highly topical area of "drugging" the shallow surface sites of protein−protein interactions. A molecule which could access the active site optimally and also bridge across to access a second binding site could be an exceptionally potent CA II inhibitor. We have recently demonstrated a similar effect in a CA II−ligand complex, wherein a steroid-derived aryl sulfamate ester with a pendant pyridin-3-ylmethyl group (STX237) was cocrystallized. This inhibitor has an IC_{50} of 0.1 nM against CA II, which was rationalized as being due, at least in part, to extra hydrophobic interactions of the pendant group with residues Gly-131, Val-134, and Leu-203 and a weak hydrogen bond (3.24 Å) between its pyridyl N-atom and Nε2 of Gln-135. In this case the pendant pyridin-3-ylmethyl group binds to a different part of the active site funnel to any of the second inhibitor binding sites identified. Inhibitor **6** is another, albeit lower affinity, example where there are interactions of a pendant group (in this case the triazole ring) with CA II. Interestingly, the triazole ring is positioned close to the second inhibitor **6** binding site so inhibitor **6** appears to be a reasonable starting point for the design of an inhibitor targeting interactions to both the second inhibitor binding and the Zn(II) ion in the active site.

The "two-prong" inhibitors mentioned above are another example of studies that have been investigating increasing affinity of inhibitors for CA II by maximizing interactions with other regions of CA II in addition to the interaction with the active site zinc. Such inhibitors contain benzenesulfonamide and IDA-Cu^{2+} groups, which were designed such that the IDA-Cu^{2+} group targets solvent-exposed histidine residues, and were shown to interact with His-64 of CA II (*45*). Another example had the aim of maximizing interactions with the surface of the protein using oligopeptidyl "tails" tethered to an arenesulfonamide group (*46*).

The oligopeptidyl "tails" interact with the hydrophobic region that forms one side of the active site funnel and is the same region that interacts with the steroid-based inhibitors from this study.

Over the past decade there has been significant interest in the development of dynamic combinatorial chemistry (DCC) techniques, and carbonic anhydrase inhibitor development was the first exemplification of the idea that virtual combinatorial library assembly in the presence of a protein could lead to the selection of high-affinity binding candidates (*47*−*49*). This process for inhibitor formation would effectively result in something similar to the "two-prong" inhibitors in that different sections of the inhibitor would interact with different regions of the protein giving the inhibitor a higher affinity for the enzyme than its constituent parts, with the selection of the best combination of constituents directed by the enzyme structure. One such study produced an inhibitor that interacted with the active site zinc and the hydrophobic side of the active site funnel (*48*). Thus, this present study reveals further evidence for the existence of a second binding site proximal to the normal CA ligand binding site and opens up the possibility of design-based ligand enhancement that could increase affinity.

CONCLUSION

The studies detailed herein offer further information on the binding of steroid sulfamate-based inhibitors in the active site of CA II. These can bind to the active site zinc through either the 3-*O*-sulfamate or 17-*O*-sulfamate groups, and there is a difference in the orientation of the steroid ring structure between these two modes of binding. When a steroid-based molecule contains both 3-*O*- and 17-*O*-sulfamate groups, the choice of which would provide the most favorable interaction with the zinc is dependent on the rest of the steroid structure. In particular, substituents on the 2-position of the A-ring lower the affinity of binding through the 3-*O*-sulfamate group, probably by steric hindrance, causing the molecule to favor binding via the 17-*O*-sulfamate group. This provides further information on how some structural elements of steroid sulfamate-based inhibitors affect affinity for CA II and offers some insights in how to make use of CA II binding to increase bioavailability for drugs targeted against other enzymes such as steroid sulfatase.

The CA II complexes with inhibitors **3** and **5** crystallize in the $P2_12_12_1$ space group, and they both contain the second zinc binding site which has been observed in other CA II structures that crystallize in the $P2_12_12_1$ space group. The CA II complex with inhibitor **6** crystallizes in the $P2_1$ space group and, as with other CA II structures that crystallize in this space group, it only contains the active site zinc. In contrast, the CA II complex with inhibitor **4** crystallizes in the $P2_1$ space group, but it does contain a second zinc bound in the same site as observed in the $P2_12_12_1$ space group structures.

The CA II structures in complex with both inhibitor **5** and inhibitor **6** show two molecules of each inhibitor bound, with the second inhibitor binding site being at the entrance to the active site funnel in the same region as that observed for the second inhibitor molecule bound in the CA II/2-MeOE2bisMATE complex structure. This demonstrates that this second site is not unique for 2-MeOE2bisMATE and, since this site is observed with different types of inhibitor in crystals with different space groups and with no interaction from symmetry-related molecules, it is possible that inhibitors could bind to this region in solution albeit at a lower affinity than in the usual active site binding. Ligand−protein interaction at this site appears to be feasible using both hydrophobic interaction of this protein with ring systems including the biphenyl motif, highly common in drug design, and hydrogen bonding with the polar sulfamate motif. The location of this second site at the entrance to the active site funnel suggests the intriguing possibility of developing high-affinity bidentate inhibitors which interact with both binding sites simultaneously. Additionally, of the second binding sites identified, this second site is closest to the active site and is therefore a more attractive region to target for bidentate inhibitors. Approaches for designing such inhibitors could be by linking together two molecules of 2-MeOE2bisMATE, inhibitors **4** or **6**, using pendant groups targeted to this region, or by using DCC techniques such that the enzyme structure influences the structure of the highest affinity inhibitor. This has not only the potential of developing high-affinity inhibitors but also the possibility of producing more selective drugs against the CA II isoenzyme.

ACKNOWLEDGMENT

We acknowledge the SRS at Daresbury (U.K.) and DESY, Hamburg (Germany), for synchrotron beam time. We thank Professor C. Fierke (University of Michigan) for the generous gift of plasmid pACA and Mr. R. Pederick for purifying human recombinant CA II.

SUPPORTING INFORMATION AVAILABLE

One figure depicting binding of inhibitors **3**, **4**, **5**, and **6** in the active site of human CA II showing $2|F_o| - |F_c|$ (blue) and $|F_o| - |F_c|$ (green) simulated annealing omit maps contoured at 1.0σ and 3.0σ, respectively. This material is available free of charge via the Internet at http://pubs.acs.org.

REFERENCES

1. Maren, T. H. (1988) The kinetics of HCO_3-synthesis related to fluid secretion, pH controls and CO_2 elimination. *Annu. Rev. Physiol. 50*, 695–717.
2. Casini, A., Scozzafava, A., Mincione, F., Menabuoni, L., Starnotti, M., and Supuran, C. T. (2003) Carbonic anhydrase inhibitors: Topically acting antiglaucoma sulfonamides incorporating esters and amides of 3- and 4-carboxybenzolamide. *Bioorg. Med. Chem. Lett. 13*, 2867–2873.
3. Recacha, R., Costanzo, M. J., Maryanoff, B. E., and Chattopadhyay, D. (2002) Crystal structure of human carbonic anhydrase II complexed with an anti-convulsant sugar sulphamate. *Biochem. J. 361*, 437–441.
4. Supuran, C. T. (2003) Carbonic anhydrase inhibitors in the treatment and prophylaxis of obesity. *Expert Opin. Ther. Pat. 13* 1545–1550.
5. Abbate, F., Winum, J.-Y., Potter, B. V. L., Casini, A., Montero, J.-L., Scozzafava, A., and Supuran, C. T. (2004) Carbonic anhydrase inhibitors: X-ray crystallographic structure of the adduct of human isozyme II with EMATE, a dual inhibitor of carbonic anhydrase and steroid sulfatase. *Bioorg. Med. Chem. Lett. 14*, 231–234.
6. Ho, Y. T., Purohit, A., Vicker, N., Newman, S. P., Robinson, J. J., Leese, M. P., Ganeshapillai, D., Woo, L. W. L., Potter, B. V. L., and Reed, M. J. (2003) Inhibition of carbonic anhydrase II by steroidal and non-steroidal sulphamates. *Biochem. Biophys. Res. Commun. 305*, 909–914.
7. Supuran, C. T., Scozzafava, A., and Casini, A. (2003) Carbonic anhydrase inhibitors. *Med. Res. Rev. 23*, 146–189.
8. Hilvo, M., Tolvanen, M., Clark, A., Shen, B., Shah, G. N., Waheed, A., Halmi, P., Hänninen, M., Hämäläinen, J. M., Vihinen, M., Sly, W. S., and Parkkila, S. (2005) Characterization of CA XV, a new GPI-anchored form of carbonic anhydrase. *Biochem. J. 392*, 83–92.
9. Türeci, Ö., Sahin, E., Vollmar, E., Siemer, S., Göttert, E., Seitz, G., Parkkila, A.-K., Shah, G. N., Grubb, J. H., Pfreundschuh, M., and Sly, W. S. (1998) Human carbonic anhydrase XII: cDNA cloning, expression, and chromosomal localization of a carbonic anhydrase gene that is over-expressed in some renal cell cancers. *Proc. Natl. Acad. Sci. U.S.A. 95*, 7608–7613.

10. Loncaster, J. A., Harris, A. L., Davidson, S. E., Logue, J. P., Hunter, R. D., Wycoff, C. C., Pastorek, J., Ratcliffe, P. J., Stratford, I. J., and West, C. M. L. (2001) Carbonic anhydrase (CA IX) expression, a potential new intrinsic marker of hypoxia: Correlations with tumor oxygen measurements and prognosis in locally advanced carcinoma of the cervix. *Cancer Res. 61*, 6394–6399.
11. Wykoff, C. C., Beasley, N. J. P., Watson, P. H., Turner, K. J., Pastorek, J., Sibtain, A., Wilson, G. D., Turley, H., Talks, K. L., Maxwell, P. H., Pugh, C. W., Ratcliffe, P. J., and Harris, A. L. (2000) Hypoxia-inducible expression of tumor-associated carbonic anhydrases. *Cancer Res. 60*, 7075–7083.
12. Howarth, N. M., Purohit, A., Reed, M. J., and Potter, B. V. L. (1994) Estrone sulfamates: Potent inhibitors of estrone sulfatase with therapeutic potential. *J. Med. Chem. 37*, 219–221.
13. Purohit, A., Williams, G. J., Roberts, C. J., Potter, B. V. L., and Reed, M. J. (1995) *In vivo* inhibition of oestrone sulphatase and dehydroepiandrosterone sulphatase by oestrone-3-*O*-sulphamate. *Int. J. Cancer 63*, 106–111.
14. Newman, S. P., Foster, P. A., Ho, Y. T., Day, J. M., Raobaikady, B., Kasprzyk, P. G., Leese, M. P., Potter, B. V. L., Reed, M. J., and Purohit, A. (2007) The therapeutic potential of a series of orally bioavailable anti-angiogenic microtubule disruptors as therapy for hormone-independent prostate and breast cancers. *Br. J. Cancer 97*, 1673–1682.
15. MacCarthy-Morrogh, L., Townsend, P. A., Purohit, A., Hejaz, H. A. M., Potter, B. V. L., Reed, M. J., and Packham, G. (2000) Differential effects of estrone and estrone-3-*O*-sulfamate derivatives on mitotic arrest, apoptosis, and microtubule assembly in human breast cancer cells. *Cancer Res. 60*, 5441–5450.
16. Purohit, A., Woo, L. W. L., Barrow, D., Hejaz, H. A. M., Nicholson, R. I., Potter, B. V. L., and Reed, M. J. (2001) Non-steroidal and steroidal sulfamates: New drugs for cancer therapy. *Mol. Cell. Endocrinol. 171*, 129–135.
17. Reed, M. J., Purohit, A., Woo, L. W. L., Newman, S. P., and Potter, B. V. L. (2005) Steroid sulfatase: Molecular biology, regulation, and inhibition. *Endocr. Rev. 26*, 171–202.
18. Stanway, S. J., Purohit, A., Woo, L. W. L., Sufi, S., Vigushin, D., Ward, R., Wilson, R. H., Stanczyk, F. Z., Dobbs, N., Kulinskaya, E., Elliott, M., Potter, B. V. L., Reed, M. J., and Coombes, R. C. (2006) Phase I study of STX 64 (667 coumate) in breast cancer patients: The first study of a steroid sulfatase inhibitor. *Clin. Cancer Res. 12*, 1585–1592.
19. Woo, L. W. L., Howarth, N. M., Purohit, A., Hejaz, H. A. M., Reed, M. J., and Potter, B. V. L. (1998) Steroidal and non-steroidal sulfamates as potent inhibitors of steroid sulfatase. *J. Med. Chem. 41*, 1068–1083.
20. Purohit, A., Williams, G. J., Howarth, N. M., Potter, B. V. L., and Reed, M. J. (1995) Inactivation of steroid sulfatase by an active site-directed inhibitor, estrone 3-*O*-sulfamate. *Biochemistry 34*, 11508–11514.
21. Elger, W., Schwarz, S., Hedden, A., Reddersen, G., and Schneider, B. (1995) Sulfamates of various estrogens are prodrugs with increased systemic and reduced hepatic estrogenicity at oral application. *J. Steroid Biochem. Mol. Biol. 55*, 395–403.
22. Ireson, C. R., Chander, S. K., Purohit, A., Perera, S., Newman, S. P., Parish, D., Leese, M. P., Smith, A. C., Potter, B. V. L., and Reed, M. J. (2004) Pharmacokinetics and efficacy of 2-methoxyoestradiol and 2-methoxyoestradiol-bis-sulphamate *in vivo* in rodents. *Br. J. Cancer 90*, 932–937.
23. Leese, M. P., Leblond, B., Smith, A., Newman, S. P., DiFiore, A., DeSimone, G., Supuran, C. T., Purohit, A., Reed, M. J., and Potter, B. V. L. (2006) 2-Substituted estradiol bis-sulfamates, multitargeted antitumor agents: Synthesis, in vitro SAR, protein crystallography, and in vivo activity. *J. Med. Chem. 49*, 7683–7696.
24. Lloyd, M. D., Pederick, R. L., Natesh, R., Woo, L. W. L., Purohit, A. P., Reed, M. J., Acharya, K. R., and Potter, B. V. L. (2005) Crystal structure of human carbonic anhydrase II at 1.95 Å resolution in complex with 667-coumate, a novel anti-cancer agent. *Biochem. J. 385*, 715–720.
25. Lloyd, M. D., Thiyagarajan, N., Ho, Y. T., Woo, L. W. L., Sutcliffe, O. B., Purohit, A., Reed, M. J., Acharya, K. R., and Potter, B. V. L. (2005) First crystal structures of human carbonic anhydrase II in complex with dual aromatase-steroid sulfatase inhibitors. *Biochemistry 44*, 6858–6866.
26. Woo, L. W. L., Jackson, T., Putey, A., Cozier, G., Leonard, P., Acharya, K. R., Chander, S. K., Purohit, A., Reed, M. J., and Potter, B. V. L. (2010) Highly potent first examples of dual aromatase−steroid sulfatase inhibitors based on a biphenyl template. *J. Med. Chem. 53*, 2155–2170.
27. Leese, M. P., Hejaz, H. A. M., Mahon, M. F., Newman, S. P., Purohit, A., Reed, M. J., and Potter, B. V. L. (2005) A-ring-substituted estrogen-3-*O*-sulfamates: Potent multitargeted anticancer agents. *J. Med. Chem. 48*, 5243–5256.
28. Armstrong, J. M., Myers, D. V., Verpoorte, J. A., and Edsall, J. T. (1966) Purification and properties of human carbonic anhydrases. *J. Biol. Chem. 241*, 5137–5149.
29. Otwinowski, Z., and Minor, W. (1997) Processing of X-ray diffraction data collected in oscillation mode, in Methods in Enzymology (Carter, C. W. J., and Sweet, R. M., Eds.) pp 307−326, Academic Press, New York.
30. McCoy, A. J., Grosse-Kunstleve, R. W., Adams, P. D., Winn, M. D., Storoni, L. C., and Read, R. J. (2007) Phaser crystallographic software. *J. Appl. Crystallogr. 40*, 658–674.
31. Eriksson, A. E., Jones, T. A., and Liljas, A. (1988) Refined structure of human carbonic anhydrase II at 2.0 Å resolution. *Proteins 4*, 274–282.
32. Brünger, A. T., Adams, P. D., Clore, G. M., DeLano, W. L., Gros, P., Grosse-Kunstleve, R. W., Jiang, J.-S., Kuszewski, J., Nilges, N., Pannu, N. S., Read, R. J., Rice, L. M., Simonson, T., and Warren, G. L. (1998) Crystallography and NMR system (CNS): A new software system for macromolecular structure determination. *Acta Crystallogr. D54*, 905–921.
33. Brunger, A. T. (2007) Version 1.2 of the crystallography and NMR system. *Nat. Protocols 2*, 2728–2733.
34. Korostelev, A., Bertram, R., and Chapman, M. S. (2002) Simulated-annealing real-space refinement as a tool in model building. *Acta Crystallogr., Sect. D 58*, 761–767.
35. Emsley, P., and Cowtan, K. (2004) Coot: Model-building tools for molecular graphics. *Acta Crystallogr. D60*, 2126–2132.
36. Kleywegt, G. (2007) Crystallographic refinement of ligand complexes. *Acta Crystallogr., Sect. D 63*, 94–100.
37. Abbate, F., Casini, A., Owa, T., Scozzafava, A., and Supuran, C. T. (2004) Carbonic anhydrase inhibitors: E7070, a sulfonamide anticancer agent, potently inhibits cytosolic isozymes I and II, and transmembrane, tumour-associated isozyme IX. *Bioorg. Med. Chem. Lett. 14*, 217–223.
38. Ippolito, J. A., Nair, S. K., Alexander, R. S., Kiefer, L. L., Fierke, C. A., and Christianson, D. W. (1995) Structure of His94→Asp carbonic anhydrase II in a new crystalline form reveals a partially occupied zinc binding site. *Protein Eng. 8*, 975–980.
39. Alexander, R. S., Kiefer, L. L., Fierke, C. A., and Christianson, D. W. (1993) Engineering the zinc binding site of human carbonic anhydrase II: Structure of the His-94→Cys apoenzyme in a new crystalline form. *Biochemistry 32*, 1510–1518.
40. Thea, S., Cevasco, G., Guanti, G., and Williams, A. (1986) The anionic sulphonylamine mechanism in the hydrolysis of aryl sulphamates. *J. Chem. Soc., Chem. Commun.*, 1582–1583.
41. Nussbaumer, P., Winiski, A. P., and Billich, A. (2003) Estrogenic potential of 2-alkyl-4-(thio)chromenone 6-*O*-sulfamates: Potent inhibitors of human steroid sulfatase. *J. Med. Chem. 46*, 5091–5094.
42. Sahm, U. G., Williams, G. J., Purohit, A., Hidalgo Aragones, M. I., Parish, D., Reed, M. J., Potter, B. V. L., and Pouton, C. W. (1996) Development of an oral formulation for oestrone 3-*O*-sulphamate, a potent sulphatase inhibitor. *Pharm. Sci. 2*, 17–20.
43. Nair, S. K., Ludwig, P. A., and Christianson, D. W. (1994) Two-site binding of phenol in the active site of human carbonic anhydrase II: Structural implications for substrate association. *J. Am. Chem. Soc. 116*, 3659–3660.
44. Kim, C.-Y., Chandra, P. P., Jain, A., and Christianson, D. W. (2001) Fluoroaromatic-fluoroaromatic interactions between inhibitors bound in the crystal lattice of human carbonic anhydrase II. *J. Am. Chem. Soc. 123*, 9620–9627.
45. Jude, K. M., Banerjee, A. L., Haldar, M. K., Manokaran, S., Roy, B., Mallik, S., Srivastava, D. K., and Christianson, D. W. (2006) Ultrahigh resolution crystal structures of human carbonic anhydrases I and II complexed with "two-prong" inhibitors reveal the molecular basis of high affinity. *J. Am. Chem. Soc. 128*, 3011–3018.
46. Cappalonga Bunn, A. M., Alexander, R. S., and Christianson, D. W. (1994) Mapping protein-peptide affinity: Binding of peptidylsulfonamide inhibitors to human carbonic anhydrase II. *J. Am. Chem. Soc. 116*, 5063–5068.
47. Ramström, O., and Lehn, J.-M. (2002) Drug discovery by dynamic combinatorial libraries. *Nat. Rev. Drug Discov. 1*, 26–36.
48. Huc, I., and Lehn, J.-M. (1997) Virtual combinatorial libraries: Dynamic generation of molecular and supramolecular diversity by self-assembly. *Proc. Natl. Acad. Sci. U.S.A. 94*, 2106–2110.
49. Poulsen, S.-A., and Bornaghi, L. F. (2006) Fragment-based drug discovery of carbonic anhydrase II inhibitors by dynamic combinatorial chemistry utilizing alkene cross metathesis. *Bioorg. Med. Chem. 14*, 3275–3284.